A Three-Dimensional Model of Canine Cardiac Ventricular Wall Electrophysiology

AP Benson[1], OV Aslanidi[2], H Zhang[2], AV Holden[1]

[1]Computational Biology Laboratory, Institute of Membrane and Systems Biology, University of Leeds, Leeds, UK
[2]Biological Physics Group, School of Physics and Astronomy, University of Manchester, Manchester, UK

Abstract

We have developed a three-dimensional computational wedge model of canine cardiac ventricular wall electrophysiology that incorporates biophysically detailed, spatially heterogeneous excitation, and high-resolution geometry and fibre orientation.

Isolated cell model electrophysiological characteristics reproduce the experimentally observed characteristics under control conditions, and under conditions of bradycardia, with the application of a class III antiarrhythmic drug, and during simulation of long-QT syndrome 2.

Propagation of excitation through the ventricular wall and the subsequent dispersion of repolarisation also reproduce experimentally observed behaviour under the same four conditions. The model therefore provides a tool for the computational study of the mechanisms underlying cardiac arrhythmias.

1. Introduction

Cardiac arrhythmias such as ventricular tachycardia and fibrillation are a major cause of morbidity and mortality in the developed world. Computational models of cardiac (nodal, atrial, Purkinje, ventricular) cells and tissues provide tools for examining the mechanisms underlying the onset of arrhythmias and interventions aimed at either preventing this onset or restoring normal sinus rhythm. They give extremely useful insight into the mechanisms of normal and pathological cell and tissue function as the data they provide can be dissected in time and space, and by parameters.

Here we present a three-dimensional wedge model of canine cardiac ventricular wall electrophysiology that incorporates biophysically detailed, spatially heterogeneous excitation equations, and high-resolution geometry and fibre orientation. Transmural activation and repolarisation in the model is examined under control conditions, during bradycardia, with the application of the class III antiarrhythmic drug d-sotalol, and during simulated long-QT syndrome 2 (LQT2).

2. Methods

Parameters in the Hund-Rudy canine epicardial cell electrophysiology model [1] were altered to model differences in isolated endocardial, midmyocardial (M) and epicardial cell current densities and kinetics, Ca^{2+} transients, and action potentials (APs), their duration (APD) and rate dependence. Maximal conductances and fluxes were scaled with respect to epicardial values according to published experimental estimates: the late Na^+ current $I_{\mathrm{Na,L}}$ by 1.15 and 1.7 for endocardial and M cells respectively; the transient outward K^+ current I_{to1} by 0.5 and 1.0; the slow delayed rectifier K^+ current I_{Ks} by 0.9 and 0.3; the Na^+-Ca^{2+} exchanger current I_{NaCa} by 0.4 and 0.5; and the Ca^{2+} uptake flux J_{up} by 0.6 and 0.7. The time course of reactivation of I_{to1} was modelled by altering the slow inactivation time constant to give values of 390, 456 and 264 ms at -80 mV in endocardial, M and epicardial cells respectively. The activation time constant of the M cell rapid delayed rectifier K^+ current I_{Kr} was twice that in epicardial and endocardial cells at all membrane potentials.

Geometry and fibre orientation of the left ventricular free wall wedge was digitally extracted from a diffusion tensor magnetic resonance imaging (DT-MRI) dataset of the canine ventricles [2]. The resolution of the reconstructed geometry is 0.39 mm^3, with the extracted wedge having dimensions of approximately $20 \times 15 \times 20$ mm. Endocardial, M and epicardial regions were assigned to the geometry so that each occupied approximately one third of the transmural distance.

Excitation in the wall was modelled using the non-linear cable equation, a reaction-diffusion-type parabolic partial

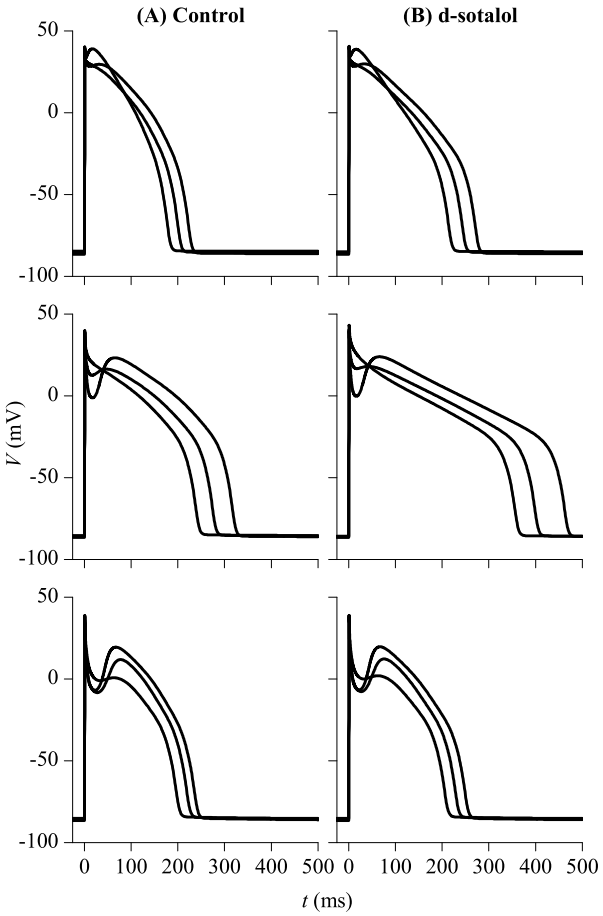

Figure 1. Computed endocardial (top), M (middle) and epicardial (bottom) steady-state APs at cycle lengths of 500, 800 and 2000 ms under control conditions (left) and with the simulated application of d-sotalol (right)

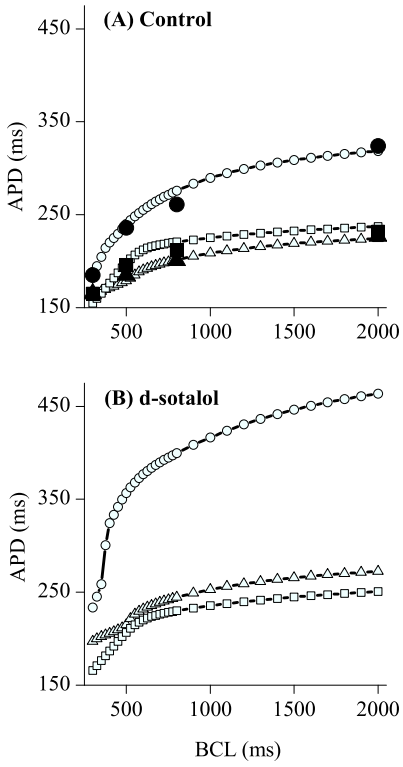

Figure 2. (A) Computed steady-state APD restitution (open symbols) and experimental data (filled symbols). (B) Computed steady-state APD restitution with the simulated application of d-sotalol. Triangles, endocardial; circles, M; squares, epicardial.

differential equation:

$$\frac{\partial V}{\partial t} = \nabla(\mathbf{D}\nabla V) - I_{\text{ion}} \ , \qquad (1)$$

where ∇ is a spatial gradient operator, $\mathbf{D}$ is a 3×3 diffusion tensor to represent electrotonic spread of voltage through the tissue, and I_{ion} is total membrane current density (μA/μF) given by one of the three cell models. $\mathbf{D}$ is a function of fibre orientation and was determined from the DT-MRI data, where diffusion was set to 0.1 and 0.06 mm^{2}ms^{-1} along and across the fibre axis, respectively. Pacing was via a twice-threshold stimulus current applied to the endocardial surface to approximate the near-synchronous activation of the ventricular myocardium by the Purkinje fibre system. Equation (1) was solved with a forward time centred space method using a time step of $\Delta t = 0.1$ ms, and a space step of $\Delta x = \Delta y = \Delta z = 0.39$ mm as defined by the DT-MRI geometry. The model was coded in C, parallelised under openMP and run locally on a Sun Fire 6800 machine utilising 24 Sun 750 MHz UltraSPARC III 64-bit processors.

We compared transmural activation and repolarisation in the ventricular wall model to the results of Akar *et al.* [3] using the same four conditions used in their experimental study: (1) pacing at a basic cycle length (BCL) of 500 ms as a control; (2) pacing at a BCL of 2000 ms to simulate bradycardia; (3) pacing at a BCL of 500 ms with the simulated effects of the I_{Kr} blocker d-sotalol, a class III antiarrhythmic drug; and (4) pacing at a BCL of 2000 ms with the simulated effects of d-sotalol in order to reproduce the effects of LQT2 [3, 4]. The effects of d-sotalol were simulated with differential block of I_{Kr} by 50% in endocardial, 70% in M and 20% in epicardial cells in order to reproduce the relative AP and APD rate adaptation effects obtained experimentally in isolated cells [5]. In each case, initial conditions for the model state variables of the excitation equations in the wedge were taken from steady-state values in single cell models.

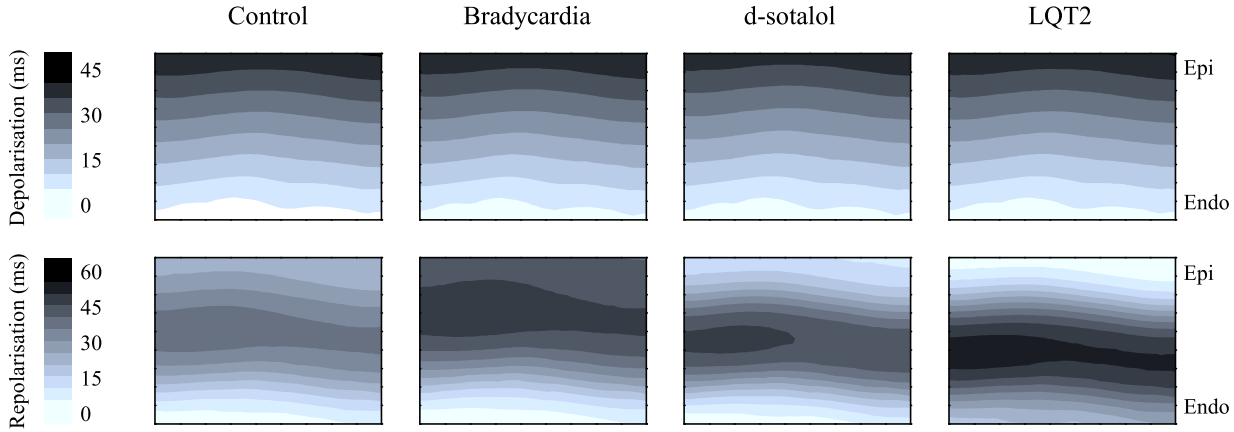

Figure 3. Transmural depolarisation (top) and repolarisation (bottom) maps for a transmural slice through the three-dimensional canine ventricular wall model. Depolarisation time was measured as the time of maximum dV/dt relative to the time of stimulus application. Repolarisation time was measured as the time of 90% repolarisation relative to the time of the first occurance of repolarisation. The four conditions are pacing at BCL = 500 ms (Control), pacing at BCL = 2000 ms (Bradycardia), pacing at BCL = 500 ms with the simulated application of d-sotalol (d-sotalol), and pacing at BCL = 2000 ms with the simulated application of d-sotalol (LQT2). Epi, epicardium; Endo, endocardium.

3. Results

Isolated myocyte model APs under control conditions (Figure 1A) agree with experimentally recorded canine APs [6], the simulated epicardial APs having the characteristic spike-and-dome morphology that decreases with decreasing BCL. This spike-and-dome morphology is absent in endocardial cells. APD restitution under control conditions also agrees with experimentally determined measures (Figure 2A, experimental data from [6]). The M cell APD is greater than both the endocardial and epicardial APD at all BCLs, with the APD restitution curve being steeper in the M cell – an increase of 130 ms between BCLs of 300 and 2000 ms compared to increases of 61 and 83 ms in endocardial and epicardial cells, respectively.

The relative changes to isolated myocyte AP morphology (Figure 1B), APD and APD restitution (Figure 2B) in the three cell types after the simulated application of d-sotalol follow the changes seen experimentally in isolated cells [5]. d-sotalol causes a greater increase of APD in M cells compared to endocardial or epicardial cells, particularly at longer BCLs, resulting in a further steepening of the M cell APD restitution curve. The endocardial APD increase with d-sotalol is greater than that of the epicardial cell at all BCLs, resulting in the endocardial curve shifting above the epicardial curve.

Depolarisation times (time of maximum dV/dt) and repolarisation times (time of 90% repolarisation) in the three-dimensional wedge model are shown for a transmural slice through the ventricular wall in Figure 3. Transmural propagation of the excitation wavefront takes approximately 40 ms under control conditions, and does not significantly differ during conditions of bradycardia, d-sotalol application, or a combination of the two to simulate LQT2 (Figure 3, top). Transmural dispersion of repolarisation, however, is greatly affected by bradycardia, simulated d-sotalol application or LQT2 (Figure 3, bottom). Under control conditions, transmural dispersion of repolarisation is 37 ms, increasing to 40, 47 and 52 ms with bradycardia, d-sotalol and LQT2, respectively. The maximum local gradient of repolarisation ($\nabla \mathrm{R}_{\mathrm{max}}$, calculated in the slice as the spatial gradient of repolarisation times) increased from 17 ms/mm under control conditions to 21, 26 and 25 ms/mm with bradycardia, d-sotalol and LQT2, respectively.

4. Discussion and conclusions

The single cell APs, APD and APD restitution all reproduce experimental measures. The epicardial cells display a characteristic spike-and-dome morphology that decreases with decreasing BCL due to the long recovery from inactivation of the transient outward K^+ current I_{to1} that is responsible for phase 1 repolarisation. The spike-and-dome morphology is absent in endocardial cells due to the decreased density of I_{to1}. APD is greatest in M cells at all BCLs, while epicardial cells have a longer APD than endocardial cells at all BCLs above 350 ms due to the increased I_{to1} causing phase 1 repolarisation and, therefore, a greater driving force for the L-type Ca^2 current $I_{\mathrm{Ca,L}}$, which re-

sults in the dome of the morphology and a prolongation of the AP. APD restitution is steepest in the M cell, resulting in proportionally greater APD in M cells at longer BCLs and, therefore, under conditions such as bradycardia.

Simulation of the application of d-sotalol also reproduces experimentally observed behaviour in isolated cells. The differential effects of d-sotalol on endocardial, M and epicardial cells [3, 5] cause a steepening of the M cell APD-rate relation, and a shift of the endocardial cell APD rate adaptation curve above that of the epicardial cell.

The effects of transmural heterogeneity of electrophysiology and simulated drug application in the three-dimensional wedge model can be seen in the activation and repolarisation maps in Figure 3. The transmural depolarisation times are not significantly altered under control conditions, bradycardia, sotalol application or simulated LQT2. However, the differential effects of rate dependence and d-sotalol, particularly on M cells, causes an increase in the transmural dispersion of repolarisation and $\nabla \mathrm{R}_{\max}$ in bradycardia, sotalol and LQT2 compared to control. This increase in the dispersion of repolarisation provides an electrophysiological substrate for reentrant arrhythmias, and has been shown experimentally to favour torsade de pointes in a wedge extracted from the canine left ventricular free wall [3]. The three-dimensional ventricular wall model presented here qualitatively reproduces this increase in the dispersion of repolarisation, and so the model is ideal for the computational study of the mechanisms underlying such cardiac arrhythmias.

Although one-dimensional models have previously been used as computationally tractable simulations of the transmural propagation of excitation through the ventricular wall, this propagation is dependent on fibre orientation, being fastest in the fibre long-axis direction. Orientation of the fibres rotates with transmural distance [2], and so this fibre orientation causes a rotational anisotropy of propagation. Inclusion of fibre orientation into three-dimensional models to be used to study arrhythmias is necessary due to the effects of this rotational anisotropy on the breakdown of the spiral waves that underlie ventricular tachycardia, into the spatially chaotic excitation characteristic of ventricular fibrillation [7]. The geometry used to construct the model presented here was obtained using DT-MRI, the data from which was then used to determine the fibre orientation [2] and corresponding rotational anisotropy at a high spatial resolution.

In conclusion, our three-dimensional model of canine cardiac ventricular wall electrophysiology incorporates biophysically detailed, spatially heterogeneous excitation, and high-resolution geometry and fibre orientation. Isolated cell APs, APD and APD rate dependence reproduce experimentally observed behaviour under control conditions, as well as during bradycardia, with the simulated application of a class III antiarrhythmic drug, and during simulated LQT2. In the ventricular wall wedge model, transmural dispersion of activation and repolarisation matches experimental results in the four conditions. The model therefore provides a tool for the computational study of the mechanisms underlying ventricular arrhythmias.

Acknowledgements

This work was supported by the European Union through the Network of Excellence BioSim, contract No. LSHB-CT-2004-005137, and grants from the Engineering and Physical Sciences Research Council and the Biotechnology and Biological Sciences Research Council, both UK. Alan Benson was supported by a Medical Research Council UK priority area research studentship in computational biology.

References

[1] Hund TJ, Rudy Y. Rate dependence and regulation of action potential and calcium transient in a canine cardiac ventricular cell model. Circulation 2004;110:3168–3174.

[2] Benson AP, Li P, Hsu EW, Holden AV. Reconstruction and visualisation of cardiac ventricular geometry and architecture from diffusion tensor magnetic resonance imaging. J Physiol 2005;567P:PC11.

[3] Akar FG, Yan GX, Antzelevitch C, Rosenbaum DS. Unique topographical distribution of M cells underlies reentrant mechanism of torsade de pointes in the long-QT syndrome. Circulation 2002;105:1247–1253.

[4] Shimizu W, Antzelevitch C. Sodium channel block with mexiletine is effective in reducing dispersion of repolarization and preventing torsade de pointes in LQT2 and LQT3 models of the long-QT syndrome. Circulation 1997; 96:2038–2047.

[5] Sicouri S, Moro S, Litovsky S, Elizara MV, Antzelevitch C. Chronic amiodarone reduces transmural dispersion of repolarization in the canine heart. J Cardiovasc Electrophysiol 1997;8:1269–1279.

[6] Liu DW, Gintant GA, Antzelevitch C. Ionic bases for electrophysiological distinctions among epicardial, midmyocardial, and endocardial myocytes from the free wall of the canine left ventricle. Circ Res 1993;72:671–687.

[7] Clayton RH, Holden AV. Dynamics and interaction of filaments in a computational model of re-entrant ventricular fibrillation. Phys Med Biol 2002;47:1777–1792.

Address for correspondence:

Professor Arun V. Holden

Institute of Membrane and Systems Biology, Worsley Building, Faculty of Biological Sciences, University of Leeds, Leeds LS2 9JT, UK

a.v.holden@leeds.ac.uk